Available online at www.sciencedirect.com
SCIENCE DIRECT®
Journal of Solid State Chemistry 177 (2004) 3768–3775
JOURNAL OF SOLID STATE CHEMISTRY
www.elsevier.com/locate/jssc

High-pressure structural behavior of $GdAlO_3$ and $GdFeO_3$ perovskites

N.L. Ross*, J. Zhao, R.J. Angel

Crystallography Laboratory, Department of Geosciences, Virginia Polytechnic Institute and State University, Blacksburg, VA 24061, USA

Received 19 May 2004; received in revised form 1 July 2004; accepted 4 July 2004
Available online 27 August 2004

Abstract

The orthorhombic perovskites, $GdAlO_3$ and $GdFeO_3$, have been studied using single-crystal X-ray diffraction up to 8.52 and 8.13 GPa, respectively, in a diamond anvil cell at 298 K. The evolution of the structures of $GdAlO_3$ and $GdFeO_3$ involves compression of both the GdO_{12} and the octahedral (AlO_6 and FeO_6) sites. The compression of the GdO_{12} site is anisotropic in both perovskites, with the four longest Gd–O distances compressing more than the eight shorter Gd–O bond lengths, resulting in a decrease in the distortion of GdO_{12} with pressure. In $GdAlO_3$, the GdO_{12} site is less compressible than the AlO_6 site, resulting in an increase of both the interoctahedral Al–O1–Al and Al–O2–Al angles with increasing pressure. Thus $GdAlO_3$ perovskite becomes less distorted with increasing pressure. In $GdFeO_3$, the GdO_{12} site displays a similar compressibility as the FeO_6 site, with little change in the Fe–O2–Fe angle with pressure but an increase of the Fe–O1–Fe tilting angle. Thus $GdFeO_3$ perovskite becomes less distorted with increasing pressure, but the change is not as pronounced as $GdAlO_3$. The high-pressure behavior of $GdAlO_3$ and $GdFeO_3$ is similar to orthorhombic $YAlO_3$ perovskite but contrasts with orthorhombic $CaSnO_3$, which becomes more distorted with increasing pressure.

Keywords: $GdAlO_3$; $GdFeO_3$; Perovskite; Structures; High-pressure; X-ray diffraction

1. Introduction

The orthorhombic $GdFeO_3$-type perovskites (*Pbnm*), with general stoichiometry ABO_3, are derived from the ideal cubic structure (*Pm3m*) via the titling and distortion of the BO_6 octahedra, as shown in Fig. 1 (e.g. Refs. [1–3]). The perovskites are of great interest in materials science because the relatively simple crystal structure displays many diverse electric, magnetic, piezoelectric, optical, catalytic, and magnetoresistive properties. In addition, perovskites are of interest in earth science because (Mg, Fe)SiO_3 transforms to a perovskite structure with *Pbnm* symmetry at high pressures and temperatures and is believed to form the bulk of the Earth's lower mantle (e.g. Ref. [4]). Studies of $GdFeO_3$-type perovskites at high pressure therefore provide a useful probe to understand atomistic controls of structural changes.

Both $GdFeO_3$ and $GdAlO_3$ perovskite are *Pbnm* perovskites, but with differing degrees of distortion from the ideal cubic structure. The greater distortion of $GdFeO_3$ relative to $GdAlO_3$ is reflected in the observed tolerance factor, $t_{obs} = \langle A{-}O\rangle/\sqrt{2}\langle B{-}O\rangle$, where $\langle A\text{–}O\rangle$ and $\langle B\text{–}O\rangle$ are the mean interatomic separations between twelve and six nearest neighbors for the *A* and *B* sites, respectively [5]. For a cubic perovskite, $t_{obs} = 1$ but $GdAlO_3$ has $t_{obs} = 0.986$ [6], similar to $CaTiO_3$ perovskite [7], and $GdFeO_3$ has $t_{obs} = 0.977$ [6], similar to $MgSiO_3$ perovskite. The equations of state of $GdAlO_3$ and $GdFeO_3$ perovskite have been determined at room temperature (298 K) using high-pressure single-crystal X-ray diffraction [6]. The reported third-order Birch–Murnaghan equation of

*Corresponding author.
E-mail address: nross@vt.edu (N.L. Ross).

0022-4596/$ - see front matter © 2004 Elsevier Inc. All rights reserved.
doi:10.1016/j.jssc.2004.07.002

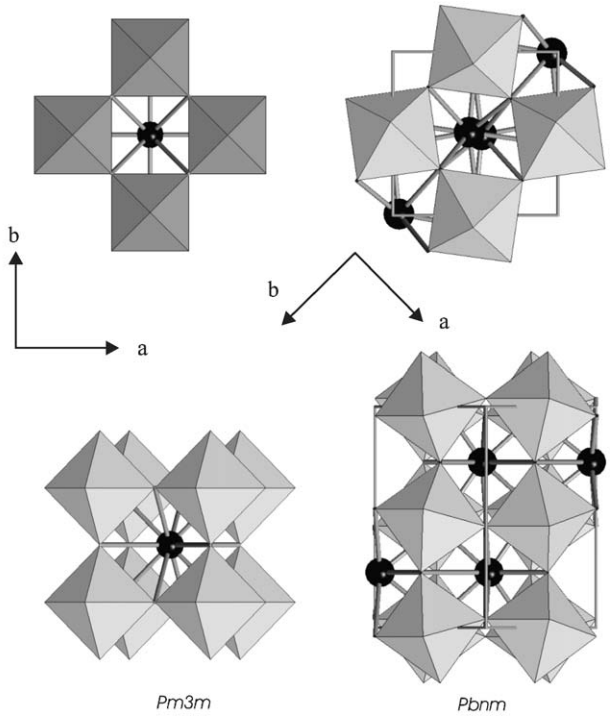

Fig. 1. Polyhedral representation of (a) cubic perovskite with *Pm3m* symmetry and (b) orthorhombic perovskite with *Pbnm* symmetry. The "*A*" cation is shown as a sphere.

state for $GdAlO_3$ has parameters of $K_{T0} = 191(1)$ GPa and $K'_0 = 5.8(3)$ compared to $K_{T0} = 182(1)$ GPa and $K'_0 = 6.3(3)$ for $GdFeO_3$. Analysis of the unit-cell parameter data showed that [100] is least compressible in both compounds and that $GdFeO_3$ compresses more isotropically than $GdAlO_3$. While there is no significant change in the pseudo-cubic unit cell parameters with pressure in $GdFeO_3$, they appear to converge in $GdAlO_3$. In particular, a_c and b_c are predicted to merge by 12 GPa, signifying a possible transition from orthorhombic to tetragonal symmetry [6].

Because the compression mechanism in perovskite is largely related to pressure-induced distortions in the AO_{12} and BO_6 sites that influence the octahedral tilting (e.g. Ref. [8]), it is critical that individual bond lengths be determined with increasing pressure. However, as pointed out by O'Keeffe et al. [9], the changes in distortion of a perovskite under even 10 GPa of pressure change are expected to be small—they estimated about 1° of tilt—and this was for a long time beyond the achievable precision of even single-crystal diffraction methods at high pressures. Recently, several improvements have been made to attempt to reduce the experimental uncertainties and systematic errors in high-pressure determination to the level approaching those obtained from crystals in air. This has enabled the evolution of distortion and tilting of polyhedra in relatively stiff materials including $YAlO_3$ [10] and $CaSnO_3$ [11] to be determined up to pressures of 8 GPa. These studies have also shown that perovskites that exhibit similar distortions from the cubic aristotype at ambient pressure may evolve very differently when subjected to even quite modest pressures.

We report here the structures of $GdAlO_3$ and $GdFeO_3$ perovskite at high pressure and we address the questions of how the tilting and distortion of the AlO_6 and FeO_6 octahedra change with pressure, the atomistic factors that control relative compressibility of the GdO_{12} and octahedral sites, and how these affect the overall changes in the distortion of the structure.

2. Experimental methods

Synthetic $GdAlO_3$ and $GdFeO_3$ samples were kindly supplied by the Division of Mineralogy, Smithsonian Museum. Single crystals for structural study were selected after X-ray diffraction measurements in air that confirmed that no twinning was obviously present. Experimental details of high-pressure structure determinations are given below.

A $GdAlO_3$ plate with dimensions of 178×178 μm was oriented as close as parallel to (110) and polished to ~30 μm thickness in order to gain access to the maximum number of reflections along the crystallographic axes. Similarly, a (110) plate of $GdFeO_3$ with dimensions 155×130 μm was polished to ~32 μm thickness. Each crystal was loaded with (110) parallel to the surface of a 600 μm anvil of an ETH diamond anvil cell [12] and a 4:1 methanol:ethanol mixture served as the pressure-transmitting medium. A 200 μm-thick T301 steel gasket was preindented to a thickness of 100 μm for $GdAlO_3$ and 110 μm $GdFeO_3$ and holes of $\phi = 440$ and 328 μm, respectively, were drilled in the center of the indented gasket. A ruby sphere was loaded into the cavity to serve as a pressure calibrant [13]. Intensity data for all accessible reflections in $GdAlO_3$ were collected at ambient pressure (in the DAC) and at 1.49(1), 2.47(2), 3.71(3), 5.17(3), 6.49(2), 7.62(2) and 8.52(3) using ω scans with the fixed-ϕ mode [14] from 2° to 40° in θ on an Xcalibur diffractometer (Mo$K\alpha$, 50 kV, 40 mA). Intensity data for $GdFeO_3$ were collected at ambient pressure (in the DAC) and at 1.01, 1.99, 3.43, 4.55, 5.94, 6.92, 7.58 and 8.13 GPa using the same conditions as $GdAlO_3$. Unit cell parameters at these pressures were also measured on a Huber four-circle diffractometer using the 8-position-centering technique [14] and these were used in the structure refinements. The pressures calculated from the equation of state [6] are in good agreement with those measured with the ruby fluorescence method. We determined the offset of the crystal from the rotation axis of the goniometor by measuring between 20 and 40 strong low-angle reflections and calculating the crystal offsets from the reflection

positions with the integration program of Angel WinIntegrStp 3.4 software [15]. We found that it was critical to eliminate these offsets by adjusting the DAC on the goniometer before data collection. Peak fitting and integration of intensities were carried out by using the WinIntegrStp 3.4 software. Other corrections such as absorption effects of DAC, including correction of beryllium plates, diamond anvils, shadowing by the gasket and the sample itself, were made by using ABSORB 6.0 [16]. After the crystallographically equivalent reflections were averaged, the remaining independent reflections with ($F > 4\sigma(F)$) were used to refine structures with RFINE99, a development version RFINE4 [17]. Details of the refinements are given in Tables 1 and 2, the refined positions of atoms and displacement parameters are given in Tables 3 and 4.

3. Results and discussion

Fig. 2a shows the variation of the Al–O bond lengths in $GdAlO_3$, $R_{ij}(P)$, with increasing pressure. Slopes of the bond lengths (dR_{ij}/dP) were obtained from a linear least-squares fitting and the linear compressibilities of the individual bonds were calculated using the relationship, $\beta R_{ij} = -1/R_{ij(0)} \times dR_{ij}/dP$ where $R_{ij(0)}$ is the value of R_{ij} at ambient pressure. The Al–O21 and Al–O22 bond lengths have similar compressibilities of 0.00172(15) and 0.00183(13) GPa^{-1}, whereas the shorter bond Al–O1 is slightly less compressible, 0.00162(7) GPa^{-1}. As a consequence, the degree of distortion due to compression of bond lengths within the AlO_6 octahedra shows a slight decrease with pressure, which is consistent with the calculated the bond-length distortion $\Delta_i = 1/n \times \sum\{(R_{ij}-R_{av})/R_{av}\}^2 \times 10^3$ (R_{av} is the average bond

Table 1
Refinement information for $GdAlO_3$ perovskite at high pressures

P (GPa)	0.0001	1.49(1)	2.47(2)	3.71(3)	5.17(3)	6.49(2)	7.62(2)	8.52(3)
N[a]	718	709	691	634	640	637	629	636
N[b]	223	223	218	214	221	211	204	206
R_{int}[c]	0.016	0.016	0.016	0.018	0.019	0.022	0.019	0.023
G_{fit}[d]	1.18	1.16	1.10	1.06	1.09	0.97	1.03	0.98
Ext ($\times 10^{-4}$)	0.144(7)	0.143(8)	0.159(8)	0.158(8)	0.155(8)	0.145(8)	0.160(9)	0.156(9)
N_{av}[e]	206	208	202	195	200	196	189	189
R_w[f]	0.023	0.023	0.023	0.024	0.026	0.026	0.024	0.027
R_{uw}[g]	0.018	0.019	0.017	0.020	0.020	0.023	0.021	0.024

[a]Number of reflections with $I > 2I_0/\sigma(I_0)$.
[b]Number of independent reflections with $F > 4\sigma(F)$.
[c]Internal residual on F (number of averaged reflections).
[d]Estimated standard deviation of unit weight observation.
[e]Weight $= (\sigma_i^2(F_i) + p^2F_i^2)^{-2}$.
[f]Weighted $R_w = [\sum w(|F_o|-|F_c|)^2/\sum|F_o|^2]^{1/2}$.
[g]Unweighted $R_{uw} = \sum||F_o|-|F_c||/\sum|F_o|$.

Table 2
Refinement information for $GdFeO_3$ perovskite at high pressures

P (GPa)	0.0001	1.01(3)	1.99(7)	3.43(3)	4.55(8)	5.94(4)	6.92(6)	7.58(4)	8.13(5)
N_{obs}[a]	794	788	783	778	784	807	779	769	752
N_{ind}[b]	318	310	313	304	298	312	307	305	291
R_{int}[c]	0.015	0.019	0.021	0.021	0.021	0.019	0.020	0.022	0.022
G_{fit}[d]	0.95	0.97	0.91	0.88	0.98	0.96	0.93	0.94	0.88
N_{av}[e]	288	295	289	283	281	293	281	280	269
Ext ($\times 10^{-4}$)	0.100(4)	0.092(6)	0.089(5)	0.090(5)	0.094(6)	0.106(5)	0.098(5)	0.100(6)	0.113(5)
R_w[f]	0.018	0.020	0.021	0.019	0.022	0.020	0.020	0.021	0.19
R_{uw}[g]	0.018	0.020	0.021	0.020	0.023	0.020	0.022	0.023	0.20

[a]Number of reflections with $I > 2I_0/\sigma(I_0)$.
[b]R_{int}, Number of independent reflections with $F > 4\sigma(F)$.
[c]Internal residual on F (number of averaged reflections).
[d]Estimated standard deviation of unit weight observation.
[e]Number of averaged reflections.
[f]Weighted $R_w = [\sum w(|F_o|-|F_c|)^2/\sum|F_o|^2]^2$.
[g]Unweighted $R_{uw} = \sum||F_o|-|F_c||/\sum|F_o|$.

Table 3
Unit cell parameters, refined positional parameters and anistropic temperature factors (β_{ij}) and equivalent isotopic temperature factors (B_{eq}) of $GdAlO_3$ perovskite at high pressure

P (GPa)	0.0001	1.49(1)	2.47(2)	3.71(3)	5.17(3)	6.49(2)	7.62(2)	8.52(3)
a (Å)	5.2537(1)	5.2421(2)	5.2359(2)	5.2278(2)	5.2186(3)	5.2111(3)	5.2046(2)	5.1999(2)
b (Å)	5.3039(1)	5.2858(1)	5.2748(1)	5.2615(2)	5.2461(2)	5.2330(2)	5.2223(2)	5.2136(1)
c (Å)	7.4435(2)	7.4292(1)	7.4180(1)	7.4041(1)	7.3883(2)	7.3744(2)	7.3625(1)	7.3533(1)
V (Å^3)	207.414(9)	205.852(7)	204.872(7)	203.655(8)	202.29(1)	201.10(1)	200.107(7)	199.347(7)
Gd[a]								
x	−0.00822(6)	−0.00801(7)	−0.00780(7)	−0.00752(7)	−0.00724(8)	−0.00714(8)	−0.00694(8)	−0.00677(8)
y	0.03770(8)	0.03658(8)	0.03585(8)	0.03498(10)	0.0339(1)	0.0330(1)	0.0323(1)	0.0316(1)
B_{eq}	0.43(1)	0.43(1)	0.46(1)	0.48(1)	0.45(2)	0.45(2)	0.45(2)	0.49(2)
$\beta 11$	0.0043(3)	0.0039(3)	0.0040(3)	0.0044(3)	0.0033(3)	0.0036(3)	0.0044(3)	0.0050(3)
$\beta 22$	0.0038(2)	0.0042(3)	0.0046(3)	0.0048(3)	0.0052(3)	0.0051(3)	0.0043(3)	0.0044(4)
$\beta 33$	0.00183(6)	0.00173(7)	0.00192(7)	0.00189(7)	0.00190(8)	0.00199(8)	0.00190(8)	0.00218(9)
$\beta 12$	−0.0006(7)	−0.00041(8)	−0.00038(8)	−0.00031(8)	−0.00035(9)	−0.00024(7)	−0.00025(8)	−0.00034(8)
Al[b]								
B_{eq}	0.36(4)	0.40(3)	0.45(4)	0.38(5)	0.44(5)	0.36(5)	0.40(5)	0.45(5)
$\beta 11$	0.003(2)	0.0036(8)	0.004(2)	0.004()	0.003(2)	0.002(2)	0.003(2)	0.003(2)
$\beta 22$	0.003(1)	0.0021(3)	0.004(1)	0.004()	0.005(2)	0.004(2)	0.003(2)	0.005(2)
$\beta 33$	0.0016(3)	−0.0002(4)	0.0020(3)	0.0015(4)	0.0020(4)	0.0017(4)	0.0024(4)	0.0021(5)
$\beta 12$	0.0001(3)	−0.0003(4)	−0.0007(4)	−0.0000(4)	0.0005(5)	0.0005(4)	0.0002(4)	−0.0003(4)
$\beta 13$	−0.0003(4)	0.0006(4)	−0.0000(4)	0.0001(4)	0.0001(4)	−0.0002(4)	0.0002(4)	−0.0002(4)
$\beta 23$	0.0000(4)	0.0036(8)	−0.0000(4)	−0.0003(4)	0.0007(4)	0.0004(4)	0.0003(4)	0.0000(5)
O1[c]								
x	0.074(1)	0.073(1)	0.071(1)	0.071(1)	0.071(1)	0.072(2)	0.071(1)	0.070(2)
y	0.486(1)	0.486(1)	0.486(1)	0.487(1)	0.491(1)	0.486(1)	0.489(1)	0.489(1)
B_{eq}	0.43(7)	0.41(8)	0.59(9)	0.47(9)	0.6(1)	0.9(1)	0.7(1)	0.6(1)
$\beta 11$	0.003(2)	0.002(4)	0.005(4)	0.007(4)	0.005(5)	0.012(5)	0.006(4)	0.001(4)
$\beta 22$	0.0052(*)	0.005(4)	0.007(4)	0.0027(4)	0.009(4)	0.009(4)	0.008(5)	0.008(4)
$\beta 33$	0.0015(7)	0.0021(7)	0.0023(6)	0.0013(7)	0.001(7)	0.0014(7)	0.0028(8)	0.0036(9)
$\beta 12$	0.0008(9)	−0.001(1)	−0.001(1)	−0.001(1)	0.001(1)	0.000(1)	−0.001(1)	−0.001(1)
O2								
x	0.7149(6)	0.7143(7)	0.7152(7)	0.7153(7)	0.7148(7)	0.7148(7)	0.7157(6)	0.7168(7)
y	0.2847(7)	0.2848(7)	0.2850(7)	0.2852(7)	0.2860(6)	0.2854(6)	0.2841(6)	0.2833(6)
z	0.0397(4)	0.0395(5)	0.0388(5)	0.0389(5)	0.0383(5)	0.0374(6)	0.0387(6)	0.0379(5)
B_{eq}	0.41(5)	0.48(6)	0.53(6)	0.50(6)	0.46(7)	0.55(7)	0.51(6)	0.45(7)
$\beta 11$	0.004(2)	0.006(3)	0.008(3)	0.005(3)	0.002(3)	0.007(3)	0.007(2)	0.004(2)
$\beta 22$	0.003(2)	0.003(2)	0.003(3)	0.005(3)	0.006(3)	0.004(3)	0.003(2)	0.003(1)
$\beta 33$	0.0019(4)	0.0019(4)	0.0021(4)	0.0017(4)	0.0021(4)	0.0022(4)	0.0021(4)	0.0018(3)
$\beta 12$	−0.0010(8)	−0.0016(8)	0.0011(8)	−0.0008(9)	−0.0018(9)	0.002(1)	−0.0006(9)	−0.0014(9)
$\beta 13$	0.0010(6)	0.0006(6)	−0.0000(6)	0.0007(7)	−0.0002(7)	0.0012(8)	0.0003(8)	0.0021(9)
$\beta 23$	−0.0007(6)	−0.0014(6)	−0.0006(6)	−0.0004(7)	−0.0015(8)	−0.0009(8)	0.0000(8)	−0.0021(8)

( ), The value from the measurement in air was used to avoid non-positive thermal parameters for O1.
[a]Y: $z = 0.25$; $\beta 13 = \beta 23 = 0$.
[b]Al: $x = 0.0$, $y = 0.5$, $z = 0.5$.
[c]O1: $z = 0.25$; $\beta 13 = \beta 23 = 0$.

length, R_{ij} is an individual bond length in the i site and n is the number of bonds) [5]. For AlO_6 in $GdAlO_3$ at ambient pressure, $\Delta_{Al} = 0.0036$ and decreases to $\Delta_{Al} = 0.005$ at 8.52 GPa. The bond-angle variance (σ) parameter [18] that is equal to zero for a regular octahedron showed a small increase from 0.59 at ambient pressure to 0.62 at 8.52 GPa.

Fig. 2b displays the variation of the Fe–O bond lengths in $GdFeO_3$ with increasing pressure. Three Fe–O bond lengths have similar linear compressibilities within the resolution of experiment with 0.00185(6) GPa^{-1} for Fe–O1, 0.00177(17) GPa^{-1} for Fe–O21, and 0.00164(17) GPa^{-1} for Fe–O22. The FeO_6 octahedra in $GdFeO_3$ are considerably more distorted than the AlO_6 in $GdAlO_3$ at room pressure, as shown by bond length distortion parameter, $\Delta_{Fe} = 0.114$, and bond angle variance parameter, $\sigma = 1.48$. The value of Δ_{Fe} at 8.13 GPa is 0.115, indicating no significant change in the bond-length distortion over the pressure range studied, but the σ decreases to 0.92 at 8.13 GPa.

Fig. 3 shows the variation of the Gd–O bond lengths in $GdAlO_3$ with increasing pressure. The compression of the GdO_{12} dodecahedral site is more anisotropic than the AlO_6 octahedron. The four longer Gd–O distances

Table 4
Unit cell parameters, refined positional parameters and anistropic temperature factors (β_{ij}) and equivalent isotopic temperature factors (B_{eq}) of $GdFeO_3$ peroskite at high pressure

P (GPa)	0.0001	1.01(3)	1.99(7)	3.43(3)	4.55(8)	5.94(4)	6.92(6)	7.58(4)	8.13(9)
a (Å)	5.3515(1)	5.3421(3)	5.3326(3)	5.3203(3)	5.3102(4)	5.2986(3)	5.2906(4)	5.2855(3)	5.2812(3)
b (Å)	5.6127(2)	5.6020(1)	5.5923(1)	5.5790(1)	5.5676(1)	5.5555(1)	5.5472(2)	5.5418(1)	5.5371(1)
c (Å)	7.6713(2)	7.6570(2)	7.6434(1)	7.6259(1)	7.6104(2)	7.5946(1)	7.5838(2)	7.5769(1)	7.5705(1)
V (Å^3)	230.42(2)	229.15(2)	227.94(1)	226.35(1)	225.00(2)	223.55(1)	222.57(2)	221.94(1)	221.38(1)
Gd[a]									
x	−0.01537(5)	−0.01545(6)	−0.01549(6)	−0.01540(6)	−0.01529(6)	−0.01534(6)	−0.01531(6)	−0.01532(6)	−0.01538(6)
y	0.06255(5)	0.06255(5)	0.06240(5)	0.06232(4)	0.06228(6)	0.06229(5)	0.06221(7)	0.06204(6)	0.06221(5)
B_{eq}	0.520(9)	0.52(1)	0.51(1)	0.50(1)	0.49(1)	0.48(1)	0.48(1)	0.48(1)	0.48(1)
$\beta 11$	0.0043(2)	0.0048(2)	0.0052(2)	0.0049(2)	0.0050(2)	0.0044(2)	0.0045(2)	0.0046(2)	0.0046(2)
$\beta 22$	0.0043(1)	0.0041(1)	0.0039(1)	0.0039(1)	0.0039(1)	0.0041(1)	0.0040(1)	0.0039(1)	0.0038(1)
$\beta 33$	0.00219(4)	0.00207(5)	0.00197(5)	0.00195(5)	0.00187(6)	0.00189(5)	0.00195(7)	0.00196(6)	0.00193(5)
$\beta 12$	−0.0005(5)	−0.00048(5)	−0.00040(5)	−0.00049(5)	−0.00052(6)	−0.00052(6)	−0.00045(6)	−0.00057(6)	−0.00040(6)
Fe[b]									
Beq	0.44(1)	0.45(2)	0.43(2)	0.425(16)	0.41(2)	0.38(2)	0.41(2)	0.39(2)	0.38(2)
$\beta 11$	0.0040(4)	0.0041(5)	0.0044(5)	0.0043(5)	0.0037(6)	0.0031(5)	0.0041(6)	0.0031(6)	0.0041(6)
$\beta 22$	0.0040(3)	0.0039(3)	0.0036(3)	0.0035(3)	0.0035(3)	0.0037(3)	0.0034(4)	0.0037(3)	0.0029(3)
$\beta 33$	0.0015(1)	0.0016(1)	0.0015(1)	0.0015(1)	0.0017(1)	0.0015(1)	0.0015(1)	0.0015(1)	0.0014(1)
$\beta 12$	0.0001(1)	−0.0000(1)	−0.0003(1)	0.0001(1)	0.0002(1)	−0.0001(1)	−0.0000(2)	0.0000(2)	0.0001(2)
$\beta 13$	0.00007(9)	−0.0001(1)	−0.0000(1)	−0.0002(1)	−0.0001(1)	0.0000(1)	0.0002(1)	0.0001(1)	−0.0001(1)
$\beta 23$	0.0002(1)	0.0003(1)	0.0001(1)	0.0001(1)	0.0000(2)	−0.0001(1)	0.0002(2)	0.0000(1)	0.0002(1)
O1[c]									
x	0.0996(8)	0.1010(9)	0.1006(9)	0.100(1)	0.099(1)	0.1001(9)	0.098(1)	0.100(1)	0.098(1)
y	0.4677(6)	0.4692(7)	0.4700(6)	0.4699(6)	0.4697(8)	0.4704(8)	0.4713(8)	0.4711(7)	0.4703(8)
B_{eq}	0.55(6)	0.68(7)	0.49(4)	0.53(6)	0.51(7)	0.47(7)	0.46(7)	0.54(7)	0.62(7)
$\beta 11$	0.004(2)	0.007(2)	0.004(2)	0.004(2)	0.005(2)	0.002(2)	0.004(3)	0.005(3)	0.005(2)
$\beta 22$	0.006(1)	0.006(1)	0.006(1)	0.006(1)	0.005(1)	0.006(1)	0.005(1)	0.007(1)	0.009(1)
$\beta 33$	0.0020(4)	0.0017(4)	0.0015(4)	0.0016(5)	0.0013(5)	0.0020(5)	0.0012(5)	0.0012(5)	0.0012(5)
$\beta 12$	−0.0001(8)	0.0003(9)	−0.0002(9)	−0.0008(9)	0.001(1)	0.000(1)	−0.000(1)	−0.001(1)	−0.002(1)
O2									
x	0.6956(6)	0.6945(6)	0.6954(6)	0.6949(6)	0.6937(6)	0.6946(6)	0.6938(6)	0.6948(6)	0.6940(6)
y	0.3012(4)	0.3009(4)	0.3009(4)	0.3010(4)	0.3011(5)	0.3016(5)	0.3018(6)	0.3014(5)	0.3016(5)
z	0.0528(3)	0.0526(3)	0.0526(3)	0.0523(3)	0.0525(4)	0.0525(3)	0.0521(4)	0.0518(3)	0.0512(3)
B_{eq}	0.60(4)	0.52(4)	0.67(5)	0.57(4)	0.56(6)	0.56(5)	0.50(5)	0.58(6)	0.39(5)
$\beta 11$	0.005(1)	0.002 (1)	0.008(2)	0.007(1)	0.005(2)	0.006(2)	0.004(2)	0.006(2)	0.004(2)
$\beta 22$	0.0051(7)	0.0061(8)	0.0046(8)	0.0035(8)	0.005(1)	0.0045(8)	0.005(1)	0.004(1)	0.0021(8)
$\beta 33$	0.0027(3)	0.0023(3)	0.0022(3)	0.0021(3)	0.0025(4)	0.0022(3)	0.0022(4)	0.0026(4)	0.0021(3)
$\beta 12$	−0.0000(6)	−0.0004(6)	−0.0005(6)	−0.0004(5)	−0.0002(6)	−0.0007(6)	−0.0001(7)	0.0003(6)	0.0001(6)
$\beta 13$	0.0011(4)	0.0007(4)	0.0002(4)	−0.0001(4)	0.0006(5)	0.0004(4)	0.0000(5)	0.0003(5)	0.0002(4)
$\beta 23$	−0.0012(3)	−0.0009(4)	−0.0005(3)	−0.0004(4)	−0.0006(5)	−0.0009(4)	−0.0014(5)	−0.0012(4)	−0.0012(4)

[a]Gd: $z = 0.25$; $\beta 13 = \beta 23 = 0$.
[b]Fe: $x = 0.0$, $y = 0.5$, $z = 0.5$.
[c]O1: $z = 0.25$; $\beta 13 = \beta 23 = 0$.

are more compressible (with an average β_{GdO} of $0.0028(2)\,GPa^{-1}$) than the eight shorter Gd–O bond distances (average β_{GdO} of $0.0010(3)\,GPa^{-1}$) and thus the distortion of GdO_{12} decreases with increasing pressure. The Δ_{Gd} decreases from 13.33 to 11.63 in the GdO_{12} polyhedron between room pressure and 8.52 GPa. The bond-angle variance (σ) parameter shows a small increase from 33.78 at room pressure to 34.22 at 8.52 GPa.

The GdO_{12} site in $GdFeO_3$ also demonstrates anisotropic compression, as shown in Fig. 4. In general, the four longer Gd–O distances are more compressible than the eight shorter Gd–O bond distances with the mean linear compressibility of the four longer Gd–O distances equal to $0.0019(1)\,GPa^{-1}$), compared to β_{GdO8} of $0.0015(1)\,GPa^{-1}$. The GdO_{12} site becomes less distorted with Δ for GdO_{12} site decreasing from 28.47 at room pressure to 27.78 at 8.13 GPa. The bond-angle variance (σ) parameter does not show any obvious variation from 32.63 at room pressure to 32.64 at 8.13 GPa.

In order to compare the relative compression of the GdO_{12} site with the AlO_6 site, the polyhedral bulk moduli, K_P, and compressibilities ($\beta = 1/K_P$) of AlO_6

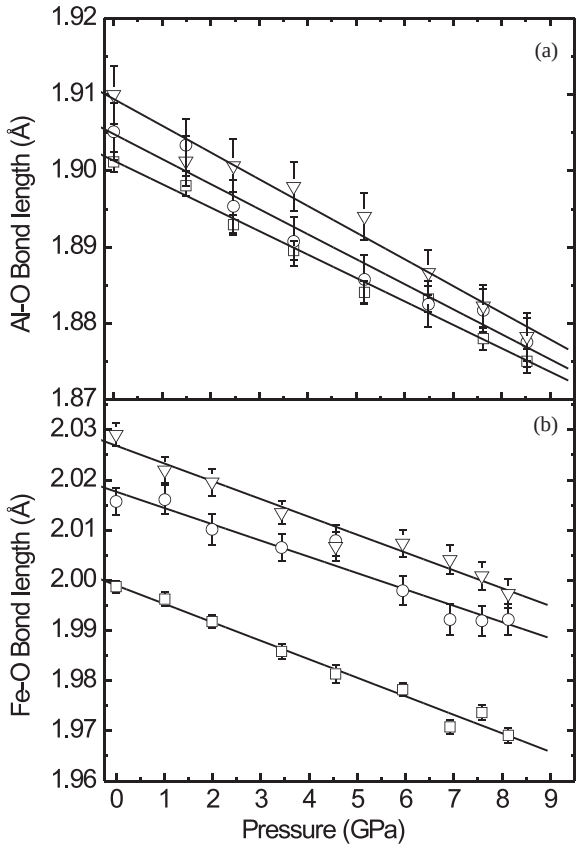

Fig. 2. The variation of (a) the Al–O bond distances in $GdAlO_3$ perovskite, Al–O1 bond (square symbols): Al–O21 bond (circle symbols) and Al–O22 (triangle symbols) and (b) the Fe–O bond distances in $GdFeO_3$ perovskite: Fe–O1 bond (square symbols), Fe–O21 bond (circle symbols) and Fe–O22 (triangle symbols) as a function of pressure.

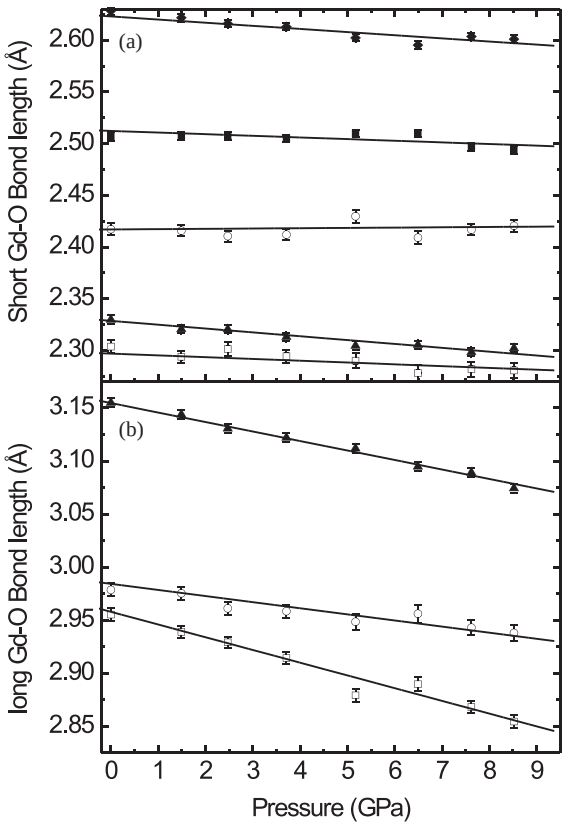

Fig. 3. (a) The variation of the eight shortest Gd–O bond lengths in $GdAlO_3$ perovskite as a function of pressure: Gd–O11 bond (hollow square symbols), Gd–O12 bond (hollow circle symbols), Gd–O21 bond (solid triangle symbols), Gd–O22 bond (solid square symbols), and Gd–O23 bond (solid diamond symbols). (b) The variation of the four longer Gd–O distances as a function of pressure: Gd–O12 bond (hollow square symbols), Gd–O14 (hollow circle symbols) and Gd–O24 (solid triangle symbols).

and GdO_{12} were obtained by fitting the polyhedral volumes with the Birch–Murnaghan finite-strain formulism:

$$P = \frac{3}{2} K_P \left[\left(\frac{V_{0,poly}}{V} \right)^{7/3} - \left(\frac{V_{0,poly}}{V} \right)^{5/3} \right] \times \left\{ 1 + \frac{3}{4}(K'_P - 4) \left[\left(\frac{V_{0,poly}}{V} \right)^{2/3} - 1 \right] \right\} \quad (1)$$

using the EOSFit v5.2 program [14], where $V_{0,poly}$ is a polyhedral volume at room pressure, K_P is the polyhedral bulk modulus, and K'_P is the first derivative with respect to pressure (assumed to be equal to 4). The resulting $V_{0,poly}$ and K_{P0} are 9.222(1) Å^3 and 179(8) GPa for AlO_6 and 42.620(26) Å^3 and 204(5) GPa for GdO_{12}. The volume compressibility of the GdO_{12} site ($\beta_{GdO12} = 1/K_P$), $\beta_{GdO12} = 0.0049(1)\,GPa^{-1}$, is therefore ~12% less than that of the AlO_6 octahedron ($\beta_{AlO6} = 0.0056(3)\,GPa^{-1}$). Polyhedral bulk moduli of FeO_6 and GdO_{12} in $GdFeO_3$ obtained from Eq. (1), assuming $K'_P = 4$, are $V_{0,poly} = 10.891(14)$ Å^3 and K_{P0} of 188(10) GPa for FeO_6 and $V_{0,poly} = 56.595(12)$ Å^3 and 187.7(18) GPa for GdO_{12}. The volume compressibility of the GdO_{12} site ($\beta_{GdO12} = 0.0053(1)\,GPa^{-1}$) is therefore the same within the experimental resolution of the FeO_6 octahedron ($\beta_{FeO6} = 0.0053(3)\,GPa^{-1}$).

As a consequence of the relative compression of the AlO_6 vs. GdO_{12} sites, the interoctahedral Al–O1–Al (α_1) and Al–O2–Al (α_2) angles both increase with increasing pressure in $GdAlO_3$ (Fig. 5a). Other angle parameters have been introduced [19,20] to describe the tilting such as the tilt of the octahedra about the pseduo-cubic $\langle 110 \rangle_p$ axis, θ, and the tilt of the of the octahedra about the pseduo-cubic $\langle 001 \rangle_p$ axis, ϕ (Fig. 5b), that are equivalent to the rotation angle, Φ, introduced by O'Keeffe et al. [9]. From Fig. 5b, we see that both ϕ and θ decrease slightly within the resolution of the measurement with pressure, which results in, for example, displacement of O1 atoms along $\langle 100 \rangle$. All tilt parameters indicate that the structure is becoming less distorted with increasing pressure.

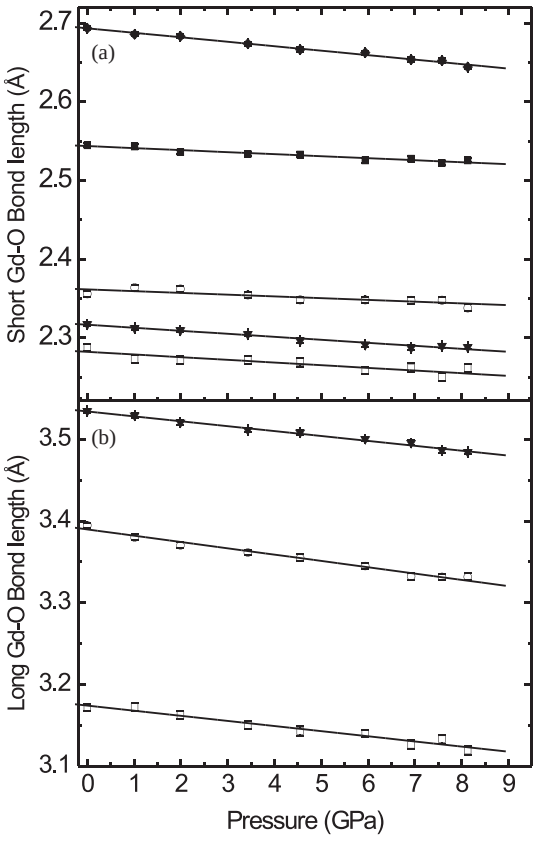

Fig. 4. (a) The variation of the eight shortest Gd–O bond lengths in $GdFeO_3$ perovskite as a function of pressure, Gd–O11 bond (hollow square symbols), Gd–O12 bond (hollow circle symbols), Gd–O21 bond (solid triangle symbols), Gd–O22 bond (solid square symbols), and Gd–O23 bond (solid diamond symbols). (b) The variation of the four longer Gd–O distances as a function of pressure, Gd–O12 bond (hollow square symbols), Gd–O14 (hollow circle symbols) and Gd–O24 (solid triangle symbols).

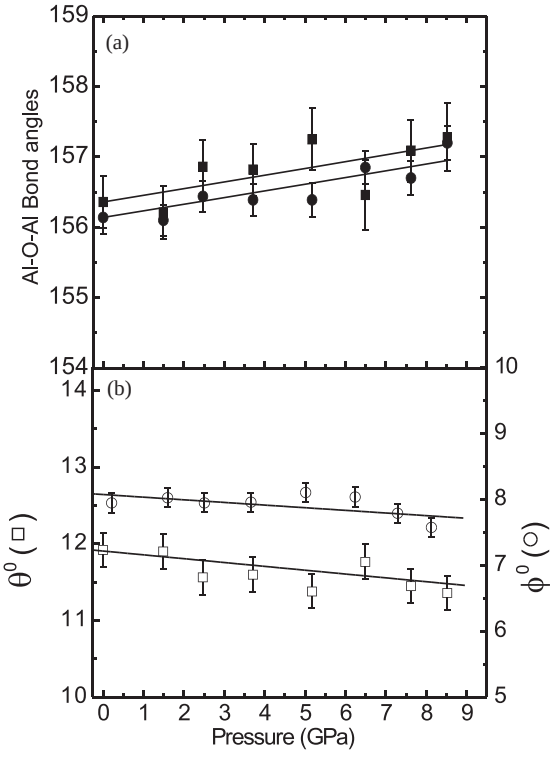

Fig. 5. Pressure evolution of (a) the octahedral tilt angles, Al–O1–Al (solid square symbols) and Al–O2–Al (solid circle symbols) of $GdAlO_3$ perovskite at high pressure, where the lines represent angles calculated using: $\alpha_i = 2a\sin[\exp(\Delta\beta_i P)\sin(\alpha_{0i}/2]$ and (b) corresponding titling angles θ and φ.

Fig. 6a shows pressure evolution of the interoctahedral angles $\angle$ Fe–O1 (4c)–Fe (α_1) and $\angle$ Fe–O2–Fe (α_2) in $GdFeO_3$ as a function of pressure. Both angles show a slight increase with pressure. The α_2 angle increases slightly with increasing pressure whereas α_1 displays a greater increase with pressure, indicating the octahedral FeO_6 tilting is mainly controlled by variation of $\angle$ Fe–O1–Fe (α_1). As shown in Fig. 6b, the corresponding tilt angle θ decreases, whereas ϕ slightly increases with pressure within the resolution of the experiment. Therefore, the octahedral tilting is mainly controlled by the angle, θ, which is closely related to the compression of bond Fe–O1 and results in displacement of O1 atoms along $\langle 100 \rangle$.

From the results, it is clear that $GdAlO_3$ displays a greater change in the degree of distortion than $GdFeO_3$, becoming less distorted than $GdFeO_3$ over a similar pressure range. This is consistent with Zhao et al.'s [22] model for prediction of high-pressure behavior in *Pbnm* perovskites. Ross et al. [6] suggested that a phase transition might occur in $GdAlO_3$ around 12 GPa on the basis of the variation of the unit cell parameters with pressure, and the structural studies of this study verify that the structure is becoming less distorted with pressure and could be approaching a phase transition. Further work is in progress to determine whether a phase transition occurs in $GdAlO_3$ perovskite at pressures in excess of 10 GPa.

4. Conclusion

The evolution of the atomic-scale structure of $GdAlO_3$ and $GdFeO_3$ involves compression of both the GdO_{12} and the AlO_6/FeO_6 sites. The compression of the GdO_{12} site is anisotropic with the four longest Gd–O distances more compressible than the eight shorter Gd–O bond lengths, and distortion within GdO_{12} decreases with pressure. The GdO_{12} site is less compressible than the AlO_6 site in $GdAlO_3$, resulting in an increase of both the Al–O1–Al and Al–O2–Al angles with increasing pressure. Thus $GdAlO_3$ perovskite becomes less distorted with increasing pressure. The GdO_{12} site displays a similar compressibility as the FeO_6 site in $GdFeO_3$, with little change in Fe–O2–Fe with pressure but an increase of the Fe–O1–Fe tilting with

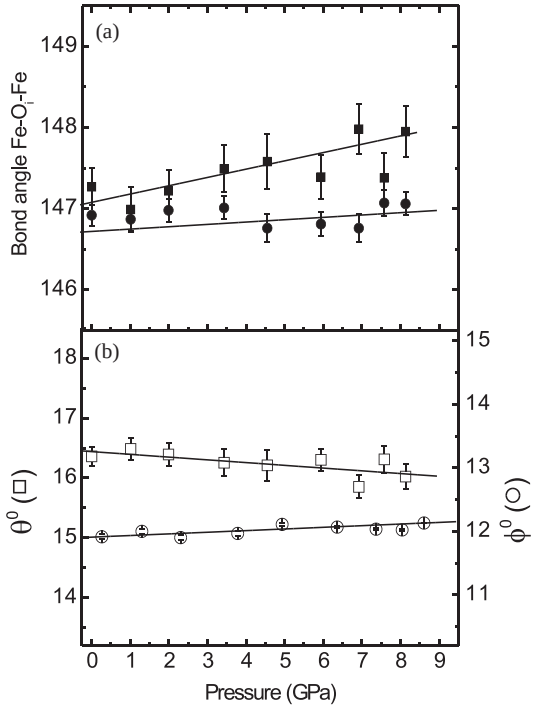

Fig. 6. Pressure evolution of (a) the octahedral tilt angles, Fe–O1–Fe (solid square symbols) and Fe–O2–Fe (solid circle symbols) of $GdFeO_3$ perovskite at high pressure, where the lines represent angles calculated using: $\alpha_i = 2a\sin[\exp(\Delta\beta_i P)\sin(\alpha_{0i}/2]$ [10,11] and (b) corresponding titling angles θ and φ.

pressure. Thus $GdFeO_3$ perovskite becomes less distorted with increasing pressure, but it is not as pronounced as $GdAlO_3$. The high-pressure behavior of $GdAlO_3$ and $GdFeO_3$ perovskite is therefore similar to $YAlO_3$ [10,21] but contrasts greatly with $CaSnO_3$, another $GdFeO_3$-type perovskite. Zhao et al. [11] found that the SnO_6 site is less compressible than the CaO_{12} site in $CaSnO_3$ and that the Sn–O–Sn angles decrease with pressure. The distortion of $CaSnO_3$ therefore increases with increasing pressure. The different response of the 3-3 and 2-4 perovskites to pressure can be ascribed to the relative compression of the AO_{12} and BO_6 sites and their high-pressure behaviors are consistent the model of Zhao et al. [22].

Acknowledgments

The authors acknowledge with gratitude the financial support for this work derived from NSF grant EAR-0105864. Ruby pressure measurements were conducted with the Raman system in the Vibrational Spectroscopy Laboratory in the Department of Geosciences at Virginia Tech. We thank Mr. Charles Farley for help with these measurements.

References

[1] A.M. Glazer, Acta Crystallogr. B 28 (1972) 3384.
[2] P.M. Woodward, Acta Crystallogr. B 53 (1997) 32.
[3] P.M. Woodward, Acta Crystallogr. B 53 (1997) 44.
[4] A. Navrotsky, D.J. Weidner, Geophysical Monograph, vol. 45, American Geophysical Union, Washington, DC, 1989.
[5] S. Sasaki, C.T. Prewitt, R.C. Liebermann, Am. Mineral. 68 (1983) 1189.
[6] N.L. Ross, J. Zhao, J. Burt, T.D. Chaplin, J. Phys.:: Condens. Matter 16 (2004) 5721.
[7] S. Sasaki, C.T. Prewitt, J.D. Bass, W.A. Shultze, Acta Crystallogr. C 43 (1987) 1168.
[8] N.L. Ross, Reviews in Mineralogy and Geochemistry, Mineralogical of Society America, Washington, DC, 2000.
[9] M. O'Keeffe, B. Hyde, J.O. Bovin, Phys. Chem. Miner. 4 (1979) 299.
[10] N.L. Ross, J. Zhao, R.J. Angel, J. Solid State Chem. 177 (2004) 1276.
[11] J. Zhao, N.L. Ross, R.J. Angel, Phys. Chem. Miner. 31 (2004) 1.
[12] D.R. Allan, R. Miletich, R.J. Angel, Rev. Sci. Instrum. 67 (1996) 840.
[13] H.K. Mao, J. Xu, P.M. Bell, J. Geophys. Res. 91 (1986) 4673.
[14] L.W. Finger, H.E. King, Am. Mineral. 63 (1978) 337.
[15] R.J. Angel, J. Appl. Crystallogr. 36 (2003) 295.
[16] R.J. Angel, J. Appl. Crystallogr. 37 (2004) 486.
[17] L. W. Finger, E. Price, US Nat Bur Stand, NBS Tech note, 854, Washington, DC.
[18] K. Robinson, G. Gibbs, P. Ribbe, Science 172 (1971) 567.
[19] Y. Zhao, D.J. Weidner, D.J. Parise, D.E. Cox, Phys. Earth Planet Interiors 76 (1993) 1.
[20] Y. Zhao, D.J. Weidner, D.J. Parise, D.E. Cox, Phys. Earth Planet Interiors 76 (1993) 17.
[21] N.L. Ross, Phase Transit. 58 (1996) 27.
[22] J. Zhao, N.L. Ross, R.J. Angel, Acta Crystallogr. B 60 (2004) 263.